Atmos. Chem. Phys. Discuss., 15, 2157–2196, 2015
www.atmos-chem-phys-discuss.net/15/2157/2015/
doi:10.5194/acpd-15-2157-2015

Atmospheric Chemistry and Physics Discussions

Temporal and spatial scaling impacts on extreme precipitation

B. Eggert[1], P. Berg[2], J. O. Haerter[3], D. Jacob[1], and C. Moseley[4]

[1]Climate Service Center 2.0, Hamburg, Germany
[2]Hydrology Research unit, SMHI, Sweden
[3]Niels Bohr Institute, Copenhagen, Denmark
[4]Max Planck Institute for Meteorology, Hamburg, Germany

Received: 1 December 2014 – Accepted: 22 December 2014 – Published: 23 January 2015

Correspondence to: B. Eggert (bastian.eggert@hzg.de)

Published by Copernicus Publications on behalf of the European Geosciences Union.

Abstract

Both in the current climate and in the light of climate change, understanding of the causes and risk of precipitation extremes is essential for protection of human life and adequate design of infrastructure. Precipitation extreme events depend qualitatively on the temporal and spatial scales at which they are measured, in part due to the distinct types of rain formation processes that dominate extremes at different scales. To capture these differences, we first filter large datasets of high-resolution radar measurements over Germany (5 min temporally and 1 km spatially) using synoptic cloud observations, to distinguish convective and stratiform rain events. In a second step, for each precipitation type, the observed data are aggregated over a sequence of time intervals and spatial areas. The resulting matrix allows a detailed investigation of the resolutions at which convective or stratiform events are expected to contribute most to the extremes. We analyze where the statistics of the two types differ and discuss at which resolutions transitions occur between dominance of either of the two precipitation types. We characterize the scales at which the convective or stratiform events will dominate the statistics. For both types, we further develop a mapping between pairs of spatially and temporally aggregated statistics. The resulting curve is relevant when deciding on data resolutions where statistical information in space and time is balanced. Our study may hence also serve as a practical guide for modelers, and for planning the space–time layout of measurement campaigns. We also describe a mapping between different pairs of resolutions, possibly relevant when working with mismatched model and observational resolutions, such as in statistical bias correction.

1 Introduction

The IPCC's fifth assessment report highlights an intensification of heavy precipitation events in North America and Europe (Hartmann et al., 2013), and projects further increase of extremes as global temperatures increase (Collins et al., 2013).

ACPD
15, 2157–2196, 2015

The study of extreme events is complex due to a strong inhomogeneity of precipitation intensities in time and space. Assessment of precipitation extremes, e.g. as defined by an intensity threshold, therefore always requires specification of the relevant temporal and spatial resolution. However, in many cases, the data resolution needed by users, observed by gauge stations or modeled by weather, respectively climate, models do not match (Willems et al., 2012).

For society, the primary interest in extreme precipitation lies in its hydrological implications, typically requiring statistics of precipitation extremes occurring at the fixed spatial area of a given catchment or drainage system. Specifically, small systems may be subject to flood risk when individual convective storm cells pass over them, while larger systems are less affected by convective-scale processes as the spatial average precipitation intensity remains low.

Relevant scales in flood risk vary enormously with the size of the area and timescales of the processes (Blöschl and Sivapalan, 1995). At the catchment scale, several hours to days are relevant, depending on the catchment area (Mueller and Pfister, 2011), whereas, e.g. urban drainage systems with scales of 1 to 10 km (Arnbjerg-Nielsen et al., 2013) are strongly impacted on scales from minutes to several hours (De Toffol et al., 2009). Even smaller temporal scales are required for research in soil erosion by water (Mueller and Pfister, 2011). A recent review article on the physical causes and impacts of rainfall extremes on different scales has been given by Westra et al. (2014).

The necessity of distinguishing scales, both in space and time, has been recognized in the past, captured e.g. by Areal Reduction Factors (ARF) and Intensity Duration Functions (IDF). Such approaches describe the decrease of average precipitation intensity due to spatial and temporal aggregation (Bacchi and Ranzi, 1996; Smith et al., 1994).

In search for adequate observational data, the capability of radar data to capture the spatial structure of storms was identified as a key factor in deriving the ARFs (Bacchi and Ranzi, 1996; Arnbjerg-Nielsen et al., 2013). A general outcome was that ARFs exhibit a decay with respect to the return period (Bacchi and Ranzi, 1996; Sivapalan

ACPD
15, 2157–2196, 2015

and Blöschl, 1998) and a dependency on the observed region, resulting from different governing rainfall generation mechanisms (Sivapalan and Blöschl, 1998).

Interestingly, early attempts at capturing intensities across scales as a simple power law dependence were found not to hold generally, as shown by Marani (2003, 2005). Instead, these papers point to a transition between an inner, a transient and an outer regime with distinct scaling: The inner regime occurs at spatial scales until around 20 km and temporal scales of 10 to 15 min while the transient regime depends on the region and season, and ends between durations of 20 to 80 h. This regime-distinction was justified in terms of scale dependent memory processes.

In the current study we recognize the fundamentally different processes in convective and stratiform precipitation. Using synoptic observation data, we classify precipitation events into convective and stratiform types. This allows us to obtain a fresh view on the aggregated statistics of these two main rain formation processes individually across scales.

Indeed, the two types of events have different physical characteristics, with convection often initiated by local radiative surface heating, resulting in a buoyantly unstable atmosphere (Houze, 1997) and stratiform precipitation stemming from large-scale frontal systems and relatively weak and uniform up-lifting. Importantly, it has been argued that the two processes may respond quite differently to temperature increases (Trenberth, 1999, 2011; Trenberth et al., 2003; Lenderink and van Meijgaard, 2008). The origin of such differential response may be especially relevant for changes resulting from anthropogenic global warming. For heavy precipitation bursts, a recent study employing observed radar signals (Berg et al., 2013) backs the differential responses. Others, using model climate projections with convection permitting simulations, point to a strong climate change signal in heavy precipitation at high temporal resolutions, and expect that a dominant contribution to extreme events will stem from convective type events (Kendon et al., 2014; Muller et al., 2011; Attema et al., 2014).

ACPD
15, 2157–2196, 2015

Hence, in spite of their small horizontal and temporal range, convective events are often found to cause severe damages to infrastructure, such as damage to buildings (Kunz, 2007; Kunz et al., 2009), or flash floods (Marchi et al., 2010).

The high demands of certain impact assessments regarding the temporal and spatial resolution of the data, go beyond the resolutions provided by typical regional climate models (RCM). As a result, climate change impact assessments for urban drainage systems typically make use of statistical downscaling of RCM data (Willems et al., 2012; Arnbjerg-Nielsen, 2012; Onof and Arnbjerg-Nielsen, 2009).

Alarmingly, different climate change signals corresponding to small and large scale events may challenge the basic assumption made in statistical downscaling procedures, namely that the empirical relationships between variables at large scales and local scales, identified for the present-day climate, would hold for periods with a warmer climate than the calibration period (Maraun et al., 2010; Wilby et al., 2004). Success then depends on the predictors chosen for the downscaling procedure and whether they are able to capture the dominant precipitation type. In most cases, only the variable itself (in this case precipitation) is employed as a predictor of sub-grid scale variability (Maraun et al., 2010). The basic assumption would then be violated.

Numerous studies have assessed the temporal and spatial characteristics of precipitation events using a storm centered approach (Austin and Houze Jr., 1972; Houze Jr. and Hobbs, 1982; Moseley et al., 2013) or from the point of view of a fixed location or area at the surface (Berndtsson and Niemczynowicz, 1988; Onof et al., 1996; Bacchi and Ranzi, 1996; Michele et al., 2001; Marani, 2003, 2005). From the storm centered, or Lagrangian, approach the lifetime and spatial extent of the storm can be analyzed. Recently, Moseley et al. (2013) applied a rain cell tracking method on radar data in order to monitor the life cycle of convective and stratiform rain events from a Lagrangian viewpoint. That study showed that at temporal scales of 30 min, convective type precipitation can produce significantly larger intensities than the stratiform type. We here originate from an observer capturing precipitation intensity over a fixed area and time

ACPD
15, 2157–2196, 2015

period. The statistics thereby constitute averages over a defined space–time window where both dry and wet sub-intervals may occur.

The different spatial and temporal scaling behavior of convective and stratiform events, as well as their different physical temperature response, raises the question, at which temporal and spatial scales convective precipitation dominates the heavy precipitation extremes. Such analysis would generate benchmarks regarding minimal climate model resolution, required for providing optimal output resolution of the respective extremes.

To this end, we here analyze high-resolution radar data (5 min temporally and 1 km spatially) over Germany for the years 2007–2008 classified by precipitation types and separated into seasons and geographic areas of Germany. Evaluation of these data over such large spatial and temporal periods allows quantification of the statistical aggregation behavior in time and space.

The structure of the article is as follows: In Sect. 2 we describe the data and methods used. Section 3 presents the results for extremes at different resolutions (Sect. 3.1) and suggests a method to compare the corresponding probability density functions (Sect. 3.2). We close with discussions and conclusions (Sect. 4).

2 Data and methods

A Germany-wide radar composite (RADOLAN-RY) from the German Weather Service is used in this study. This data set is provided on an approximate 900 km × 900 km grid with a 1 km horizontal resolution and contains information derived from 17 radar measurement facilities (Fig. 1). The rainfall rates (R) were derived from raindrop reflectivities (Z) using the Z–R relationship (Steiner et al., 2004). The data are stored as discrete instantaneous intensities with an increasing bin size towards higher values. For the analysis, the two year time period covering 2007–2008 is considered. The data have been used (Moseley et al., 2013) and compared with gauge data previously (Berg et al., 2013).

ACPD
15, 2157–2196, 2015

For the current analysis, radar grid-points are aggregated in time, i. e. $\Delta t \in \{5, 10, 15, 20, 30, 45, 60, 120, 180, 240, 360\}$ min, and in space over square gridbox areas with linear dimensions $\Delta x \in \{1, 2, 3, 4, 5, 6, 7, 8, 9, 10, 12, 15, 25, 50\}$ km. Aggregation includes all possible pairs $\{\Delta t, \Delta x\}$. Spatial aggregation is performed such that a coarser grid box starts at the bottom left corner of the domain and aggregates over the respective number of grid points towards the top right, with no overlap between the coarser grid boxes. As a consequence, the number of aggregated grid boxes scales $\sim 1/(\Delta t \Delta x^2)$. In cases where the original horizontal resolution cannot evenly be divided by the resolution of the coarser grid, the remaining grid points at the top and right border are not considered. This is the closest mimic of a gridded model.

Synoptic cloud observations from the Met Office Integrated Data Archive System (MIDAS) data base [http://badc.nerc.ac.uk/view/badc.nerc.ac.uk__ATOM__dataent_ukmo-midas] are used to separate large-scale and convective precipitation following Berg et al. (2013). The locations of the stations used are shown in Fig. 1. The classification process is carried out such that first, a classification is made for each single station and each 3 hourly observation into *convective*, *stratiform*, *mixed* or *no observations*. Second, to ensure more stable conditions, the classifications are aggregated in space to quadrants over the region (see Fig. 1), such that each quadrant contains one single classification for each 3 hourly time period. The aggregated classification can only be *convective* (*stratiform*) if there are no simultaneous observations of *stratiform* (*convective*) in the quadrant. Else, the classification will be considered to be of the *mixed* type.

For the aggregated time resolutions 5 to 180 min, the precipitation is flagged as *convective*, respectively *stratiform*, according to the corresponding 3 hourly time slice. For time resolutions longer than three hours, no mixing of *convective* and *stratiform* in the multiple time steps are allowed in the respective classes, otherwise they are classified as *mixed*. For classifications of *convective* or *stratiform* together with *mixed* conditions, the classification is performed according to the following procedure: For time resolutions 240 to 360 min at least one time slice has to be flagged as *convective* or *strati-*

ACPD
15, 2157–2196, 2015

form. This procedure was found to be the best compromise between rigid classification and sufficient data availability at the coarsest averaging windows.

Next, for each averaging window, the total number of convective and stratiform *events*, i.e. single time-steps with an intensity higher than 1 mm day^{-1}, is counted. To ensure that enough events for statistical analysis are present, the analysis is restricted to resolutions where at least 500 convective and 500 stratiform events were detected. All other fields will be marked as insufficient (gray squares in the Figs. 3, 4 and 7).

3 Results

3.1 Quantifying the impact of spatial and temporal aggregation on convective and stratiform precipitation extremes

Differential impact on exceedence probabilities. We define the cumulative distribution function (CDF) as the probability of precipitation exceeding a given intensity I:

$$\mathrm{CDF}(\Delta t, \Delta x, I) \equiv \frac{\int_I^\infty N(\Delta t, \Delta x, I')\mathrm{d}I'}{\int_{I_0}^\infty N(\Delta t, \Delta x, I')\mathrm{d}I'}, \quad (1)$$

where $N(\Delta t, \Delta x, I)$ is the number of data aggregates to resolution Δt and Δx with averaged precipitation intensity I, and I_0 is the lower measurement cutoff. In the following, we choose $I_0 = 1\,\mathrm{mm\,day^{-1}}$ throughout. $\mathrm{CDF}(\Delta t, \Delta x, I)$ thus describes the percentiles of precipitation intensity when conditioning on wet periods. Figure 2 shows $\mathrm{CDF}(\Delta t, \Delta x, I)$ for Germany for different Δt and Δx conditional on convective and stratiform events. Note the logarithmic representation of the data, i.e. the figure focuses on the high precipitation intensities between the 99.9th percentile (10^{-1}) and the 90th percentile (10^{1}) of the distribution.

It is important to realize the effect of aggregation at varying scales: Consider first spatial aggregation (see legend in Fig. 2). Convection forms patterns with intense and localized precipitation peaks, separated spatially by regions without precipitation (Austin

ACPD
15, 2157–2196, 2015

and Houze Jr., 1972; Moseley et al., 2013; Berg et al., 2013). Performing averages over areas of increasing size therefore yields broad variation of averages at small spatial scales but rapid decrease of variation as data is aggregated over larger areas. Stratiform precipitation can be thought of as a noisy pattern overlaid some average level, and sampling over small areas yields a good description of the statistics also at larger areas of aggregation.

Consider now temporal aggregation from an interval well below the convective lifetime (e.g. $\ll$ 30 min): The effect of temporal aggregation is to even out spatial variations due to the large-scale flow. This makes convection appear spatially more uniform. For stratiform precipitation, patterns are already less localized in space and temporal aggregation will change the statistics less.

We make three observations (Fig. 2) in support of this assessment: First, while convective precipitation can be much more intense (compare e.g. the solid curves in Fig. 2a vs. b) the decrease of mean intensity due to aggregation is more pronounced than for stratiform precipitation. Second, we find that the relative differences in the CDF's between the 1 and 50 km data are stronger if the data is stored at 5 min resolution than for the 360 min data. For stratiform events we find almost no differences between precipitation intensities at resolutions below 12 km for a 360 min temporal resolution. Only at the largest regions, 50 km, does the spatial aggregations clearly modify the CDF as the non-precipitating region off the boundary of the event is included. This finding suggests that, for a given time resolution, there should be an adequate horizontal resolution to store or collect data. Choosing higher spatial resolution would be unable to add more information to the statistics and fine-scale details are already averaged out temporally. This naturally also holds vice versa, when a spatial resolution is specified.

Third, we highlight the close match of the convective intensity CDF's when comparing two different datasets, namely 5 min and 50 km vs. 360 min, 1 km. For these pairs of resolutions the time aggregation has a similar statistical effect on precipitation intensities as does spatial aggregation.

ACPD
15, 2157–2196, 2015

This latter observation can be appreciated when remembering the Taylor-hypothesis of "frozen turbulence" (Taylor, 1938), stating that as the mean atmospheric flow advects eddies past a station, the properties of the eddies remain unaltered. Consider e.g. an average convective event with constant precipitation intensity over its lifetime. According to Berg et al. (2013) and Moseley et al. (2013) the average convective event has a lifetime of approximately 30 min, a spatial extent of $\sim$ 10 km and a propagation speed of $\sim 10\,\mathrm{ms}^{-1}$. When using a 50 km grid box and 5 min temporal resolution, the event will move about 3 km and thus affect roughly $\frac{10\times13}{50\times50} \approx 5\,\%$ of the cell. When an event of $\sim$ 10 km cross section moves over a location with $\sim 10\,\mathrm{m/s}$, its passage over the location would last $\sim$ 1000 s, which is $\sim$ 17 min, and $\frac{17}{360} \approx 5\,\%$ of the time.

In the following we discuss how the actual observations depart from the approximation of the Taylor-hypothesis and how this departure is influenced by the precipitation type. In reality, events change intensity also on short timescales, many events can be superimposed in space and time and the large scale flow is not constant.

To proceed, we now focus on intensity changes at a specific percentile, defined for a given combination of Δt and Δx by the inverse of Eq. (1), i.e. the intensity corresponding to a choice of exceedence probability. We return to the entire distribution functions in Sect. 3.2. Specifically, we now choose the 99th percentile of all detected precipitation events and refer to this percentile as *extreme precipitation*. This percentile was found to be a good compromise between the aim of focusing mainly on the high end of the intensity distributions and the need for sufficient data for the statistics. Using a percentile value as threshold to define precipitation extremes is a common practice in the modeling community.

For varying Δx and Δt, Figs. 3 and 4 show the 99th percentile of precipitation intensities for convective (termed $\hat{I}_{\mathrm{cv}}(\Delta t, \Delta x)$) and stratiform (termed $\hat{I}_{\mathrm{ls}}(\Delta t, \Delta x)$) events, respectively, for the entire region of Germany, and separated into North and South Germany, as well as for the whole year, and separated into the summer (April–September) and winter (October–March) seasons. Note that we used a non linear scaling for the x and y axis to better visualize the intensity changes at very high resolutions. The same

ACPD
15, 2157–2196, 2015

plots as in Figs. 3 and 4 but with linear scales are shown in the supplementary material. In the linear case the arcs, found when connecting fields with similar extreme intensities, become almost straight lines. Straight lines mean, that for any choice of a resolution pair, equivalent resolutions can be obtained by a simple linear transformation.

When comparing $\hat{I}_{cv}(\Delta t, \Delta x)$ (Fig. 3) to $\hat{I}_{ls}(\Delta t, \Delta x)$ (Fig. 4), it is striking that at high temporal and spatial resolutions, $\hat{I}_{ls}$ has only about a third as high intensities as $\hat{I}_{cv}$. However, $\hat{I}_{ls}$ shows much less spatial and seasonal differences when compared to those of $\hat{I}_{cv}$. For example, the increase in intensity at the highest resolution in summer vs. winter is about 220 % for $\hat{I}_{cv}$ and only approximately 20 % for $\hat{I}_{ls}$. This finding is in line with the relatively weak temperature response of stratiform precipitation intensities as reported recently (Berg et al., 2013).

Regionally, South Germany exhibits higher $\hat{I}_{cv}$ in summer as compared to the North. This is largely due to complex orographic areas in southern Germany, e.g. the highly convectively active area of the Black Forest in southwestern Germany (Khodayar et al., 2013).

The highest intensities of stratiform precipitation occur in North Germany in the months May to September. We find that for time durations lower than 3 h the highest intensities occur between June to August. For longer time durations, the highest intensities occur in the months September to November (see supplement).

Scaling behavior of convective and stratiform precipitation events. To quantify the reduction due to spatial aggregation, we define the area reduction factor ARF(x) as the reduction of the 99th percentile at spatial resolution x relative to spatial resolution 1 km, keeping the temporal resolution fixed at 5 min, i.e.

$$\mathrm{ARF}(x) \equiv 1 - \frac{\hat{I}(5\,\mathrm{min}, x)}{\hat{I}(5\,\mathrm{min}, 1\,\mathrm{km})}, \tag{2}$$

where $\hat{I}$ can be either $\hat{I}_{cv}$ or $\hat{I}_{ls}$. Analogously, we define the duration reduction factor DRF(t) as the reduction of $\hat{I}_{cv}$ and $\hat{I}_{ls}$ due to aggregation to the temporal resolution t

ACPD
15, 2157–2196, 2015

relative to the resolution of 5 min, keeping the spatial resolution at 1 km, i.e.

$$\mathrm{DRF}(t) \equiv 1 - \frac{\hat{I}(t, 1\,\mathrm{km})}{\hat{I}(5\,\mathrm{min}, 1\,\mathrm{km})}. \quad (3)$$

ARF and DRF are shown in Fig. 5a and b, respectively, for both precipitation types, and separately for the summer and winter season, as well as for north and south Germany. Considering $\hat{I}_{\mathrm{cv}}$, a strong intensity reduction can be seen when the horizontal (Fig. 5a) or temporal (Fig. 5b) resolution is decreased. The reduction due to spatial aggregation shows clear seasonal and regional differences. The lowest ARFs occur in northern Germany in winter (68 % at 50 km grid size), the highest in south Germany in summer (84 % at 50 km grid size). Temporal aggregation is nearly independent of seasonal and regional distinctions and reaches values of about 80 to 85 % at a 6 hourly resolution.

$\hat{I}_{\mathrm{ls}}$ shows much less pronounced ARF's and DRF's. For the maximum spatial aggregation, only 52 % reduction is found in north Germany in winter. The seasonal and regional differences are smaller than for the $\hat{I}_{\mathrm{cv}}$ and differ only by less than 10 percentage units. Temporal aggregation shows also only small regional and seasonal differences causing DRF's of 60 to 70 %, at a temporal resolution of 6 h.

Comparing the relevance of space compared to time aggregation. We can distinguish the behavior of spatial and temporal aggregation using two kinds of approaches (Deidda, 2000). The first approach would be to regard precipitation as self-similar process (simple scaling). In this case the Taylor-hypothesis (Taylor, 1938) would be obeyed and temporal variations can be reinterpreted as spatial variations that are advected over a fixed location by a large-scale flow, that has a constant value over the observed temporal and spatial scales.

Following the notion of "frozen turbulence", intensity change due to spatial aggregation can then be calculated from the intensity changes that result due to temporal aggregation multiplied by a constant velocity u, i.e. $\Delta x \approx \Delta t \cdot u$. This would only hold, if precipitation extremes could be seen as objects of temporally constant characteristics that are translated by large scale advection.

ACPD
15, 2157–2196, 2015

The second approach would assume that the spatial and temporal aggregation behavior of precipitation extremes would behave like a self-affine process. In this case, the simple linear relation that connects changes due to time aggregation with changes due to spatial aggregation through an advection velocity, generally does not hold anymore. A multifractal analysis is needed, where in short, the "velocity" itself would become a function of the respective spatial and temporal scales. A proper understanding of the relationship between spatial and temporal aggregation is e.g. crucial for precipitation downscaling and bias correction methods (Wood et al., 2004; Piani et al., 2010a, b).

Our goal here is to characterize the differences in scaling of convective and stratiform extremes: Comparing the intensity reduction due to time aggregation for the 1 km dataset (Fig. 3a, left column) with the intensity reduction that results from spatial aggregation at a temporal resolution of 5 min (bottom row), a 4 km spatial aggregation is comparable to that of spatial aggregation for roughly 15 min. Similarly, for stratiform precipitation (Fig. 4a) we find that 6 km spatial aggregation corresponds to 15 min temporally. There is hence a dependence on the precipitation type, a relation we now analyze.

Figure 6a shows for each horizontal resolution the matching temporal resolution that achieves similar intensity reduction. We describe the relation between temporal and spatial aggregation at a fixed Δx by

$$f_{\Delta x}(\Delta t) = \left| \hat{I}(\Delta t, 1\,\mathrm{km}) - \hat{I}(5\,\mathrm{min}, \Delta x) \right| , \quad (4)$$

We now define $\phi_{\Delta x}$ as the minimum value of $f_{\Delta x}$ w.r.t. Δt:

$$\phi_{\Delta x} = \min_{\Delta t} f_{\Delta x}(\Delta t) . \quad (5)$$

The best matching time window Δt for a given Δx can be determined using the inverse function of $f_{\Delta x}$: $\Delta t = f^{-1}(\phi)$. In practice, we determine Δt by an iterative numerical procedure, using first an interpolation between available resolutions for better approximation. The result for several high percentiles is shown for both precipitation types over

ACPD
15, 2157–2196, 2015

Germany for the entire year on a log-log plot (Fig. 6a), i.e. straight lines represented power laws. If the Taylor-hypothesis was obeyed, the exponent would equal unity.

Within the limitations of the relatively noisy data, we find that the data represents a straight line over most of the analyzed spatial range and can be fitted to a power law function $\Delta t = a \times \Delta x^b$ with fitting parameters a and b, or by using dimensionless variables (i.e. defining $\chi \equiv \Delta x / \Delta x_0$, $\tau \equiv \Delta t / \Delta t_0$ and $\widetilde{a} \equiv a \Delta x_0^b / \Delta t_0$), we have

$$\tau = \widetilde{a} \chi^b , \tag{6}$$

with fitting parameters $\widetilde{a}$ and b. The parameter $\widetilde{a}$ is a scaling parameter and describes the Δt_0 corresponding to Δx_0. χ^b describes how the relevance of space compared to the time aggregation changes with resolution.

Consider e.g. climate model simulation data. A choice often has to be made as to the proper model output resolution, i.e. the combination of time and space intervals within which an average value of an observable (say, precipitation intensity) is produced before writing data to storage. The curve described by Eq. (6) indicates, which combination of resolutions gives consistently high information with regard to both space and time. If only higher spatial resolution is chosen without changing temporal resolution, the information gain would be relatively moderate, and vice versa for exclusive temporal resolution changes. For this reason we term values on the line $\tau = \widetilde{a} \chi^b$ "optimal".

In Fig. 6a and b, the best-fit for the 99th intensity percentile is shown for convective and stratiform precipitation. We find that b is similar for both types (generally between 1.17 and 1.32), a departure from unity that should be confirmed by other data sources than the radar data at hand. An exponent $b > 1$ indicates, that extreme precipitation is self-affine (self-similarity would require $b = 1$). The fractal properties of precipitation were already highlighted in earlier studies and are found to be a result of the hierarchical structure of precipitation fields (Schertzer and Lovejoy, 1987) with cells that are embedded in small meso-scale areas which in turn occur in clusters in large-scale synoptic areas analyzed by Austin and Houze Jr. (1972).

ACPD
15, 2157–2196, 2015

Table 1 displays $\tilde{a}$ and b for the different percentiles shown in Fig. 6a (non-dimensional). We find that for convective precipitation $\tilde{a}$ is near 0.5. Within the error bars there is no obvious dependence on percentile. $\tilde{a} \sim 0.5$ indicates that temporal resolution should be approximately doubled for optimal resolution (in the sense defined above). Stratiform extreme intensities are less localized, and changes due to horizontal aggregation are lower than for the convective case. Therefore even higher temporal resolutions are required to capture intensity variations at the km scale and to create an added value compared to datasets stored on a lower horizontal resolution. For the Stratiform type we find a scaling parameter $\tilde{a} \sim 0.28$ indicating that the temporal resolution should be about 3.6 times higher resolved than in the original dataset to yield consistency between spatial and temporal information. Conversely, one could increase spatial measurement scale significantly without much loss of information.

Since the values of b are similar for both precipitation types (Table 1), the difference between the optimum temporal resolution of stratiform and convective events is kept constant over the entire analyzed range of Δx. We find that the different scaling between the two precipitation types mainly results from the varying $\tilde{a}$. The *optimal* temporal resolution for stratiform events is therefore always approximately $0.49/0.28 = 1.75$ (mean values in Table 1) times the time period that would be *optimal* for convective events. Efficiency of measurement would therefore require different priorities of space and time resolution for convective and stratiform precipitation.

Note also the kink in the observed curves in Fig. 6a, where a change of slope is observed. To show that this kink is a manifestation of the scale mismatch, we aggregate data spatially to 2 km horizontal resolution and re-plot (Fig. 6b). Due to this procedure the kink almost vanished. This test shows that aligning resolutions according to Eq. (6) allows smooth scaling.

For further analysis, and to make contact to the Taylor-hypothesis, we use the matching Δx and Δt to define a ratio describing the intensity reduction due to spatial aggregation, which we call space–time ratio (ST ratio):

$$\text{ST ratio}(\chi) \equiv \chi/\tau = \tau^{1-b}/\tilde{a}. \quad (7)$$

ACPD
15, 2157–2196, 2015

This ratio can be used to achieve approximate equivalence of spatial and temporal averaging in a similar way as in Deidda (2000) who calculated the velocities using tracking techniques. The ST ratio can now be used to generalize the Taylor-hypothesis for self-affine process, by using the ST ratio instead of a constant velocity to describe the relation between space and time. For the original Taylor-hypothesis, $b = 1$ and Eq. (7) becomes a constant. Figure 6c shows the dimensional ST ratio calculated for different Δx for the 95th, 98th, 99th and 99.9th percentile, using data without seasonal distinctions over Germany. The ST ratio lies in the same range as the velocities calculated by Deidda (2000). Low ST ratios for horizontal resolutions lower than about 2 to 4 km are again a result of the mismatch of the 5 min temporal resolution and the 1 km spatial resolution explained above. Note the deviating value of $\widetilde{a}$ for the 99.9th percentile of stratiform precipitation. This could be explained by mesoscale stratiform systems with embedded convection, i.e. systems that are somewhat intermediate between stratiform and convective events. The corresponding graph (Fig. 6c) shows intermediary behavior, connecting the curves of convective precipitation (low Δx) to those of stratiform precipitation at high Δx. Due to substantial noise at high spatial resolution it is not possible to identify if the ST ratio shows a constant behavior ($b = 1$) at the high resolutions, therefore the results in Zawadzki (1973) and Waymire et al. (1984) indicating the Taylor-hypothesis to hold for time scales less than 40 min can neither be confirmed nor rejected.

Dominance of convective vs. stratiform extremes including event occurrences. Until now we only illustrated differences in the 99th percentiles of detected convective and stratiform events with precipitation intensities above 1 mm day^{-1}, i.e. conditional probability density functions. The sample size therefore depends on the number of detections of the specific precipitation type, the resolution of the dataset and the area fraction in the detected quadrants with precipitation intensities higher than the specified threshold. Including the events without precipitation in the statistics will have a major impact on the percentile values, therefore a sensitivity analysis, performing the same analyses shown in Figs. 3 and 4 but with non conditional probability density functions

ACPD
15, 2157–2196, 2015

was done (not shown). This demonstrated, that the ST ratios are not strongly affected by this threshold. Naturally, due to the high number of non-precipitation-values, the high percentiles show correspondingly lower intensities. Table 2 indicates the event occurrences classified as convective or stratiform, in the 3 hourly synoptic observations.

To consider the strong variation in occurrences, e.g. concerning season, we find that also the relative occurrence frequency of the two types of events has to be accounted for. We again use the 99th percentile for all data above 1 mm day^{-1}, but now without distinction of precipitation type, for each aggregation interval, as well as for each region and season. In the following we re-define $\hat{I}$ as the corresponding intensity. (see Supplement for $\hat{I}$ values).

To assess the relative likelihood of a certain precipitation type to cause extreme precipitation, Fig. 7 shows the ratio of the number of convective events exceeding the intensity $\hat{I}$ vs. the total number (convective + stratiform) of events exceeding $\hat{I}$, i.e. $N_{cv}(I > \hat{I})/(N_{cv}(I > \hat{I}) + N_{ls}(I > \hat{I}))$.

However, dominance again depends on resolution: E.g., in South Germany (all year) 80–90 % of precipitation extremes are of the convective type for the higher resolutions. Only when the data is aggregated to resolutions with grid-spacings of 25 km and more, the percentage of stratiform events becomes appreciable. Even stronger differences occur between seasons: In summer, convection dominates extremes but is of less importance in winter (less than 10 % for the aggregated datasets and less than 35 % even at the very high resolution datasets).

It is important to note that we used a percentile threshold for this analysis and the corresponding intensity threshold fluctuates with seasons. To test whether our findings simply are a consequence of overall higher intensities in summer, we also compare similar intensities for summer and winter (using the 98th percentile for summer and the 99th percentile in winter, see Fig. 7g–i and supplementary material). This revealed, that seasonal differences nonetheless prevail.

Sensitivity tests using the 95th, 98th, 99th and 99.9th percentile of precipitation intensities showed, that the role of convective precipitation in the extremes increases

ACPD
15, 2157–2196, 2015

with higher percentiles, and convective precipitation becomes more relevant also over larger aggregated areas and time steps (see supplementary material). For example, Fig. 8 (all Germany) shows that at relatively low percentiles convective and stratiform events have the same exceedence probability but with increasing percentile convection dominates, especially at high spatial resolution.

3.2 Assessing PDF changes due to data aggregation

The results of Sect. 3.1 highlight the need of choosing appropriate temporal resolution when analyzing extreme precipitation events at a specified spatial scale. Vice versa, specified spatial scales have to be matched by appropriate temporal scales. Such information may translate directly to working time and equipment costs when planning adequate measurement missions in the field. For modeling, this assessment may allow for more efficient storage of simulation data and optimal use of computing resources.

To give an estimate of the information loss due to the aggregation process, we adopt a measure similar to that of the Perkins skill score (Perkins et al., 2007), originally designed to validate a model against observations by assigning a skill score. Here, we use it to quantify the overlap between two intensity PDFs at different horizontal and temporal resolutions. We define the *PDF overlap* as:

$$S(\Delta t_1, \Delta x_1; \Delta t_2, \Delta x_2) \equiv \int_{I_0}^{\infty} \min(\rho_{\Delta t_1, \Delta x_1}(I), \rho_{\Delta t_2, \Delta x_2}(I))\, dI \tag{8}$$

where I is precipitation intensity, I_0 is the measurement cutoff, $\rho_{\Delta t, \Delta x}(I)$ is the normalized PDF as in Eq. (1), and $\min(\cdot,\cdot)$ gives the minimum of the two arguments. Hence, $S(\Delta t_1, \Delta x_1; \Delta t_2, \Delta x_2)$ quantifies the overlap between PDFs of aggregated data at the spatio-temporal resolutions $(\Delta t_1, \Delta x_1)$, and $(\Delta t_2, \Delta x_2)$, respectively. If the two PDFs are identical, the overlap value is 1, if there is no overlap at all, it is 0. The PDF overlap is

ACPD
15, 2157–2196, 2015

a means of comparing not only a fixed percentile of precipitation intensity but measuring the similarity of entire distribution functions. It is hence a way to quantify our initially qualitative discussion regarding Fig. 2.

Figure 9 shows PDF overlap values for the convective precipitation intensities aggregated over Germany in three different ways: Fig. 9a shows the PDF overlap between the aggregated time resolution with the corresponding 5 min data, but at fixed horizontal resolution, i.e. $S(5\,\text{min}, \Delta x; \Delta t, \Delta x)$ at matrix element position $(\Delta t, \Delta x)$. For the spatially highly resolved data ($\Delta x < 7$ km), the PDF overlap degrades quickly when temporal resolution is reduced, while degradation is much slower at lower spatial resolution. In practice, if a defined spatial area, say a metropolitan region of 25 km is of interest, performing measurements at 60 min resolution may lead to a tolerable margin of error while a smaller region of 2 km would require 5 or 10 min temporal resolution for the same margin of error. The chart could hence be used to estimate the error when data is available at one resolution but another is of interest. In panel Fig. 9b we present an analogous analysis, but we have now fixed the temporal resolution and compare to the 1 km datasets, i.e. $S(\Delta t, 1\,\text{km}; \Delta t, \Delta x)$ at matrix element position $(\Delta t, \Delta x)$. A similar pattern emerges with degradation now occurring for decreased spatial resolution. In a third analysis (Fig. 9c) we calculate the overlap $S(60\,\text{min}, 10\,\text{km}; \Delta t, \Delta x)$ between aggregated data of spatio-temporal resolution (t, x) and the dataset at 60 min temporal resolution and 10 km spatial resolution. This reference point was chosen, because it is close to current state-of-the-art RCM simulation over Europe.

The plot shows a ridge with values close to 1, ranging from 5 min and 25 km to 120 min and 5 min resolution. Apparently, all spatio-temporal resolutions along this curve produce PDFs which differ only slightly from the 5 min, 10 km aggregation. PDF overlap values quickly decrease when departing from this ridge. Comparing this ridge with the intensity decrease in the 99th percentile as illustrated in Fig. 3a we find that the PDF overlap mirrors the changes found in the 99th percentile. Figure 9c is also shown as an example to demonstrate how the information from Fig. 9a and b can be combined

ACPD
15, 2157–2196, 2015

in order to identify at which scales precipitation data stored at a certain resolution can be applied without modifying the intensities to fit to the desired scale.

In the example the 10 km, 60 min data can be used at horizontal resolutions of about 6 to 15 km and shows also similar precipitation statistics at a temporal resolution of 45 min. The analogous analysis is presented for stratiform precipitation in Fig. 10. The PDF overlap now degrades more slowly compared to convective precipitation. The change in PDF overlap due to temporal aggregation is shown in Fig. 10a. For example, at a 50 km grid size we find that twice the temporal aggregation can be tolerated as compared to convective precipitation when a given PDF overlap is demanded. Similar conclusions hold for the degradation as function of horizontal resolution (Fig. 10b). Starting at about 20 min we again find that the Δx can be increased to about twice the value for convective events to achieve the same PDF overlap value. For the overlap $S(60\,\text{min}, 10\,\text{km}; \Delta t, \Delta x)$, shown in Fig. 10c, the lower sensitivity to resolution changes for stratiform precipitation translates to a substantial widening of the red area near the ridge, indicating much lower errors of estimating extremes at unavailable resolutions when stratiform precipitation is concerned, compare to the case for convective precipitation (Fig. 9c). Performing measurements over extended regions can already serve as a reasonable predictor of more local extremes.

4 Discussion and conclusions

Precipitation is strongly inhomogeneous in time and space. Averaging in space or time therefore transforms the distribution function. The resulting smoothening especially affects the extreme values. In this study, the focus is on how such averaging affects the two synoptically identifiable precipitation types, namely stratiform and convective precipitation. Convective events are known to produce strong and localized precipitation events while stratiform events are more homogeneous.

We separate high-resolution radar-derived precipitation intensities into convective and stratiform events, using synoptic observations and define extreme precipitation as

ACPD
15, 2157–2196, 2015

the 99th percentile of the distribution function. Unlike other studies, we here concentrate on the different aggregation behavior of the two precipitation types at different seasons and regions of Germany.

Convection more sensitive to regions and seasons. We make basic general observations regarding seasons and regions: Convective extremes were found to be markedly stronger in summer than in winter, an effect possibly explained by previously noted strong temperature response of that type (Berg et al., 2013). We also note a regional gradient, with convective extremes considerably stronger in the south than in the north of Germany in summer. This is largely due to the convectively active Black Forest region, but may also be a consequence of higher summer temperatures in the south. Stratiform extremes showed seasonal and regional differences of about 20 % with the highest values occurring in northern Germany. We then characterize intensity reduction due to temporal and spatial aggregation of extreme precipitation events. Spatially, convective extremes again show clear regional and seasonal differences: Strongest intensity reductions with spatial scale were found in south Germany in summer, the lowest in north Germany in winter. Stratiform extremes show smaller regional and seasonal differences in the reduction behavior.

Optimal pairs of resolutions. For proper choice of model output resolution, precipitation downscaling as well as bias correction, the relation between the DRF's as compared to ARF's is important. Originating from the radar data resolution of 5 min temporally and 1 km spatially, we produced sequences of aggregation, both in space and time, yielding: (i) temporally aggregated intensities for spatial scales held fixed, (ii) spatially aggregates intensity for temporal scales held fixed. Associating the respective aggregation resolution by matching the corresponding precipitation extremes, we yield pairs of temporal and spatial resolutions, which then define a curve. We show how this curve can be used to generalize the Taylor-hypothesis to the situation where temporal scales change disproportionately with spatial scales. The result e.g. allow data analysts to identify pairs (Δx, Δt) of spatial and temporal resolutions for which the decrease in extreme precipitation intensities due to temporal aggregation matches that

ACPD
15, 2157–2196, 2015

due to horizontal aggregation. Departing from the points on the graph (Fig. 6) would give only moderately increased statistical information. Interestingly, the slopes of the curves of convective and stratiform events are similar; the main scaling difference between convective and stratiform events can be described by a scaling factor. We find that in order to attain the *optimal* resolution, convective events require about 1.75 times higher horizontal resolutions at a given temporal scale than stratiform events.

Equivalently, the graph can be recast into the ratio between corresponding grid sizes and durations (which we term ST ratio). For constant ratio as function of spatial scale, the Taylor-hypothesis would be obeyed. However, the ST ratio of convective and stratiform extreme precipitation algebraically decreases with increasing Δx with similar exponents for both precipitation types.

In practice, in regional climate models the temporal output is often lower than the *optimum* resolution computed here. For example, the *optimum* temporal resolution for state of the art regional climate simulations, performed at a 11 km horizontal resolution, would be approximately 20 to 25 min. Many regional models however do not output at sub-hourly frequency and often only daily averages are stored. A higher temporal output would be advisable since this information is accessible by the model already (most models have computing time steps $\sim$ seconds – minutes) and recording at higher frequency would mainly effect storage space, not simulation run-time (assuming efficient I/O-handling).

Inclusion of dry events. The different aggregation behavior of convective and stratiform events means that the probability that an extreme precipitation event being of the convective type changes with the resolution of the data. If an intensity threshold, for example the 99th percentile, is used in a study to identify extreme events, all events lower than this threshold will be filtered out. Depending on the resolution of the dataset used in the analyses, different meteorological events will be considered as extreme. Using the 99th percentile of all precipitation events, we analyze the contribution of convective events to the total as a function of data aggregation. Knowledge of this ratio is needed for example to compare climate signals of extreme precipitation, that were calculated

ACPD
15, 2157–2196, 2015

at different resolutions. This ratio changes with resolution, season and regions of Germany. In summer and at high resolution, essentially all precipitation extremes are of the convective type. Over north Germany stratiform events contribute only at horizontal resolutions coarser than 12 km when the duration interval is kept constant to 5 min. For a higher threshold (99.9th percentile), convective events again dominate more strongly and convective extremes consequently prevail over even larger areas and durations.

PDF overlap. Changes caused by temporal aggregation depend on the spatial scale of the data and vice versa. To examine these dependencies, we compare pairs of PDFs derived for different aggregation resolutions using a method developed by Perkins et al. (2007). This leads to practical application as to choosing appropriate resolutions in time (space) when a domain of given area (time interval) is specified. For example: If measuring precipitation data at one pair of resolutions, our results indicate other pairs of resolutions that could be derived from models and should yield similar statistical distribution functions. This may be relevant for statistical bias correction.

The Supplement related to this article is available online at doi:10.5194/acpd-15-2157-2015-supplement.

Acknowledgements. The authors acknowledge the radar data from the German Weather Service (DWD). We further acknowledge the provision of station data from the British Met Office for provision of the Met Office Integrated Data Archive System (MIDAS) for the synoptic codes, retrieved through the The British Atmospheric Data Centre (BADC). B. Eggert acknowledges support from Climate Service Center 2.0, P. Berg acknowledges support from SMHI, J. O. Haerter acknowledges support from the Danish National Research Foundation through the Center for Models of Life and C. Moseley acknowledges support from the project HD(CP)^2, funded by the German Federal Ministry of Education and Research.

The service charges for this open access publication have been covered by a Research Centre of the Helmholtz Association.

ACPD
15, 2157–2196, 2015

References

Arnbjerg-Nielsen, K.: Quantification of climate change effects on extreme precipitation used for high resolution hydrologic design, Urban Water J., 9, 57–65, doi:10.1080/1573062X.2011.630091, available at: http://www.tandfonline.com/doi/abs/10.1080/1573062X.2011.630091, 2012. 2161

Arnbjerg-Nielsen, K., Willems, P., Olsson, J., Beecham, S., Pathirana, A., Bülow Gregersen, I., Madsen, H., and Nguyen, V.-T.-V.: Impacts of climate change on rainfall extremes and urban drainage systems: a review., Water Sci. Technol., 68, 16–28, doi:10.2166/wst.2013.251, available at: http://www.ncbi.nlm.nih.gov/pubmed/23823535, 2013. 2159

Attema, J. J., Loriaux, J. M., and Lenderink, G.: Extreme precipitation response to climate perturbations in an atmospheric mesoscale model, Environ. Res. Lett., 9, 014003, doi:10.1088/1748-9326/9/1/014003, 2014. 2160

Austin, P. M., and Houze Jr., R. A.: Analysis of the structure of precipitation patterns in New England, J. Appl. Meteorol., available at: http://journals.ametsoc.org/doi/abs/10.1175/1520-0450(1972)011<0926:AOTSOP>2.0.CO;2, 1972. 2161, 2164, 2170

Bacchi, B. and Ranzi, R.: On the derivation of the areal reduction factor of storms, Atmos. Res., 42, 123–135, doi:10.1016/0169-8095(95)00058-5, available at: http://linkinghub.elsevier.com/retrieve/pii/0169809595000585, 1996. 2159, 2161

Berg, P., Moseley, C., and Haerter, J. O.: Strong increase in convective precipitation in response to higher temperatures, Nat. Geosci., 6, 181–185, doi:10.1038/ngeo1731, available at: http://www.nature.com/doifinder/10.1038/ngeo1731, 2013. 2160, 2162, 2163, 2165, 2166, 2167, 2177

Berndtsson, R. and Niemczynowicz, J.: Spatial and temporal scales in rainfall analysis – Some aspects and future perspectives, J. Hydrol., 100, 293–313, available at: http://www.sciencedirect.com/science/article/pii/0022169488901898, 1988. 2161

Blöschl, G. and Sivapalan, M.: Scale issues in hydrological modelling: a review, Hydrol. Process., 9, 251–290, available at: http://onlinelibrary.wiley.com/doi/10.1002/hyp.3360090305/abstract, 1995. 2159

Collins, M., Knutti, R., Arblaster, J., Dufresne, J.-L., Fichefet, T., Friedlingstein, P., Gao, X., Gutowski, W., Johns, T., Krinner, G., Shongwe, M., Tebaldi, C., Weaver, A., and Wehner, M.: Long-term climate change: projections, commitments and irreversibility, in: Climate Change 2013: the Physical Science Basis, Contribution of Working Group I to the Fifth Assessment

ACPD
15, 2157–2196, 2015

Report of the Intergovernmental Panel on Climate Change, edited by: Stocker, T. F., Qin, D., Plattner, G.-K., Tignor, M., Allen, S. K., Boschung, J., Nauels, A., Xia, Y., Bex, V., and Midgley, P. M., Cambridge University Press, Cambridge, United Kingdom and New York, NY, USA, 2013. 2158

De Toffol, S., Laghari, A. N., and Rauch, W.: Are extreme rainfall intensities more frequent? Analysis of trends in rainfall patterns relevant to urban drainage systems., Water Sci. Technol., 59, 1769–1776, doi:10.2166/wst.2009.182, available at: http://www.ncbi.nlm.nih.gov/pubmed/19448312, 2009. 2159

Deidda, R.: Rainfall downscaling in a space-time multifractal framework, Water Resour. Res., 36, 1779–1794, doi:10.1029/2000WR900038, available at: http://doi.wiley.com/10.1029/2000WR900038, 2000. 2168, 2172

Hartmann, D., Tank, A. K., Rusticucci, M., Alexander, L., Brönnimann, S., Charabi, Y., Dentener, F., Dlugokencky, E., Easterling, D., Kaplan, A., Soden, B., Thorne, P., Wild, M., and Zhai, P.: Observations: atmosphere and surface, in: Climate Change 2013: the Physical Science Basis, Contribution of Working Group I to the Fifth Assessment Report of the Intergovernmental Panel on Climate Change, Cambridge University Press, Cambridge, United Kingdom and New York, NY, USA, 2013. 2158

Houze, R. A.: Stratiform precipitation in regions of convection: a meteorological paradox?, B. Am. Meteorol. Soc., 78, 2179–2196, doi:10.1175/1520-0477(1997)078<2179:SPIROC>2.0.CO;2, 1997. 2160

Houze Jr., R. A., and Hobbs, P. V.: Organization and structure of precipitating cloud systems, Adv. Geophys., available at: http://www.atmos.washington.edu/~gcg-dlh/MG/PDFs/ADV82_houz_organization.pdf, 1982. 2161

Kendon, E. J., Roberts, N. M., Fowler, H. J., Roberts, M. J., Chan, S. C., and Senior, C. A.: Heavier summer downpours with climate change revealed by weather forecast resolution model, Nat. Clim. Chang. 4, 1–7, doi:10.1038/NCLIMATE2258, 2014. 2160

Khodayar, S., Kalthoff, N., and Scha, G.: The impact of soil moisture variability on seasonal convective precipitation simulations. Part I: Validation, feedbacks, and realistic initialisation, Meteorologische Zeitschrift, 22, 489–505, doi:10.1127/0941-2948/2013/0403, 2013. 2167

Kunz, M.: Von Wettersystemen zu Extremereignissen: Gefährdungsanalyse über orografisch strukturiertem Gelände, Verständnis, Vorsorge und Bewältigung von Naturkatastrophen, Abschlusssymposium 2007, Graduiertenkolleg “Naturkatastrophen”, 24./25. Juli 2007, Hrsg.: S. Senitz, Universitätsverlag, Karlsruhe, 195–203, 2007. 2161

ACPD
15, 2157–2196, 2015

Kunz, M., Sander, J., and Kottmeier, C.: Recent trends of thunderstorm and hailstorm frequency and their relation to atmospheric characteristics in southwest Germany, Int. J. Climatol., 29, 2283–2297, doi:10.1002/joc.1865, available at: http://doi.wiley.com/10.1002/joc.1865, 2009. 2161

Lenderink, G. and van Meijgaard, E.: Increase in hourly precipitation extremes beyond expectations from temperature changes, Nat. Geosci., 1, 511–514, doi:10.1038/ngeo262, available at: http://www.nature.com/doifinder/10.1038/ngeo262, 2008. 2160

Marani, M.: On the correlation structure of continuous and discrete point rainfall, Water Resour. Res., 39, 1128, doi:10.1029/2002WR001456, available at: http://doi.wiley.com/10.1029/2002WR001456, 2003. 2160, 2161

Marani, M.: Non-power-law-scale properties of rainfall in space and time, Water Resour. Res., 41, W08413, doi:10.1029/2004WR003822, available at: http://doi.wiley.com/10.1029/2004WR003822, 2005. 2160, 2161

Maraun, D., Wetterhall, F., Ireson, A. M., Chandler, R. E., Kendon, E. J., Widmann, M., Brienen, S., Rust, H. W., Sauter, T., Venema, V. K. C., Chun, K. P., Goodess, C. M., Jones, R. G., Onof, C., and Vrac, M.: Precipitation downscaling under climate change: recent developments to bridge the gap between dynamical models and the end user, Rev. Geophys., 48, 1–34, doi:, 2010. 2161

Marchi, L., Borga, M., Preciso, E., and Gaume, E.: Characterisation of selected extreme flash floods in Europe and implications for flood risk management, J. Hydrol., 394, 118–133, doi:10.1016/j.jhydrol.2010.07.017, available at: http://linkinghub.elsevier.com/retrieve/pii/S0022169410004427, 2010. 2161

Michele, C. D., Kottegoda, N. T., Rosso, R., and De Michele, C.: The derivation of areal reduction factor of storm rainfall from its scaling properties, Water Resour. Res., 37, 3247–3252, doi:10.1029/2001WR000346, available at: http://doi.wiley.com/10.1029/2001WR000346, 2001. 2161

Moseley, C., Berg, P., and Haerter, J. O.: Probing the precipitation life cycle by iterative rain cell tracking, J. Geophys. Res.-Atmos., 118, 13361–13370, doi:10.1002/2013JD020868, available at: http://doi.wiley.com/10.1002/2013JD020868, 2013. 2161, 2162, 2165, 2166

Mueller, E. N. and Pfister, A.: Increasing occurrence of high-intensity rainstorm events relevant for the generation of soil erosion in a temperate lowland region in Central Europe, J. Hydrol., 411, 266–278, doi:10.1016/j.jhydrol.2011.10.005, available at: http://linkinghub.elsevier.com/retrieve/pii/S0022169411006986, 2011. 2159

ACPD
15, 2157–2196, 2015

Muller, C. J., O'Gorman, P. A., and Back, L. E.: Intensification of Precipitation Extremes with Warming in a Cloud-Resolving Model, J. Climate, 24, 2784–2800, doi:10.1175/2011JCLI3876.1, available at: http://journals.ametsoc.org/doi/abs/10.1175/2011JCLI3876.1, 2011. 2160

Onof, C. and Arnbjerg-Nielsen, K.: Quantification of anticipated future changes in high resolution design rainfall for urban areas, Atmos. Res., 92, 350–363, doi:10.1016/j.atmosres.2009.01.014, available at: http://linkinghub.elsevier.com/retrieve/pii/S0169809509000313, 2009. 2161

Onof, C., Northrop, P., Wheater, H. S., and Isham, V.: Spatiotemporal storm structure and scaling property analysis for modeling, J. Geophys. Res., 101, 26415, doi:10.1029/96JD01378, available at: http://doi.wiley.com/10.1029/96JD01378, 1996. 2161

Perkins, S. E., Pitman, A. J., Holbrook, N. J., and McAneney, J.: Evaluation of the AR4 climate models' simulated daily maximum temperature, minimum temperature, and precipitation over Australia using probability density functions, J. Climate, 20, 4356–4376, doi:10.1175/JCLI4253.1, available at: http://journals.ametsoc.org/doi/abs/10.1175/JCLI4253.1, 2007. 2174, 2179

Piani, C., Haerter, J., and Coppola, E.: Statistical bias correction for daily precipitation in regional climate models over Europe, Theor. Appl. Climatol., 99, 187–192, 2010a. 2169

Piani, C., Weedon, G., Best, M., Gomes, S., Viterbo, P., Hagemann, S., and Haerter, J.: Statistical bias correction of global simulated daily precipitation and temperature for the application of hydrological models, J. Hydrol., 395, 199–215, 2010b. 2169

Schertzer, D. and Lovejoy, S.: Physical modeling and analysis of rain and clouds by anisotropic scaling multiplicative processes, J. Geophys. Res., 92, 9693–9714, available at: http://onlinelibrary.wiley.com/doi/10.1029/JD092iD08p09693/full, 1987. 2170

Sivapalan, M. and Blöschl, G.: Transformation of point rainfall to areal rainfall: intensity-duration-frequency curves, J. Hydrol., 204, 150–167, available at: http://www.sciencedirect.com/science/article/pii/S0022169497001170, 1998. 2159, 2160

Smith, J., Bradley, A., and Baeck, M.: The space-time structure of extreme storm rainfall in the southern plains, J. Appl. Meteor., 33, 1402–1417, available at: http://dx.doi.org/10.1175/1520-0450(1994)033<1402:TSSOES>2.0.CO;2, 1994. 2159

Steiner, M., Smith, J. A., and Uijlenhoet, R.: A microphysical interpretation of radar reflectivity-rain rate relationships, J. Atmos. Sci., 61, 1114–1131, 2004. 2162

ACPD
15, 2157–2196, 2015

Taylor, G.: The spectrum of turbulence, P. R. Soc. London, 164, 476–490, available at: http://rspa.royalsocietypublishing.org/content/164/919/476.full.pdf, 1938. 2166, 2168
Trenberth, K.: Conceptual Framework for Changes of Extremes of the Hydrological Cycle with Climate Change, Weather and Climate Extremes, available at: http://link.springer.com/chapter/10.1007/978-94-015-9265-9_18, 1999. 2160
Trenberth, K.: Changes in precipitation with climate change, Clim. Res., 47, 123–138, doi:10.3354/cr00953, available at: http://www.int-res.com/abstracts/cr/v47/n1-2/p123-138/, 2011. 2160
Trenberth, K. E., Dai, A., Rasmussen, R. M., and Parsons, D. B.: The changing character of precipitation, B. Am. Meteorol. Soc., 84, 1205–1217, doi:10.1175/BAMS-84-9-1205, available at: http://journals.ametsoc.org/doi/abs/10.1175/BAMS-84-9-1205, 2003. 2160
Waymire, E., Gupta, V. K., and Rodriguez-Iturbe, I.: A spectral theory of rainfall intensity at the meso-β scale, Water Resour. Res., 20, 1453–1465, doi:10.1029/WR020i010p01453, available at: http://doi.wiley.com/10.1029/WR020i010p01453, 1984. 2172
Westra, S., Fowler, H. J., Evans, J. P., Alexander, L. V., Berg, P., Johnson, F., Kendon, E. J., Lenderink, G., and Roberts, N. M.: Future changes to the intensity and frequency of short-duration extreme rainfall, Rev. Geophys., 52, 2014RG000464, doi:10.1002/2014RG000464, available at: http://onlinelibrary.wiley.com/doi/10.1002/2014RG000464/full, 2014. 2159
Wilby, R., Charles, S., Zorita, E., and Timbal, B.: Guidelines for use of climate scenarios developed from statistical downscaling methods, 1–27, available at: http://www.narccap.ucar.edu/doc/tgica-guidance-2004.pdf, 2004. 2161
Willems, P., Arnbjerg-Nielsen, K., Olsson, J., and Nguyen, V.: Climate change impact assessment on urban rainfall extremes and urban drainage: methods and shortcomings, Atmos. Res., 103, 106–118, doi:10.1016/j.atmosres.2011.04.003, available at: http://linkinghub.elsevier.com/retrieve/pii/S0169809511000950, 2012. 2159, 2161
Wood, A. W., Leung, L. R., Sridhar, V., and Lettenmaier, D.: Hydrologic implications of dynamical and statistical approaches to downscaling climate model outputs, Climatic Change, 62, 189–216, 2004. 2169
Zawadzki, I.: Statistical properties of precipitation patterns, J. Appl. Meteorol., 12, 459–472, available at: http://journals.ametsoc.org/doi/abs/10.1175/1520-0450(1973)012%3C0459:SPOPP%3E2.0.CO;2, 1973. 2172

ACPD
15, 2157–2196, 2015

Table 1. Estimation of the exponents b and the pre-factors $\tilde{a}$ for the different convection types and percentiles together with the standard deviation of the parameter estimate. * Excluding the 99.9th percentile.

precipitation type	percentile	$\tilde{a}$	b
convective	95th	0.51 ± 0.05	1.17 ± 0.03
	98th	0.45 ± 0.03	1.25 ± 0.02
	99th	0.43 ± 0.04	1.27 ± 0.02
	99.9th	0.55 ± 0.01	1.24 ± 0.01
	mean	0.49 ± 0.03	1.23 ± 0.02
stratiform	95th	0.20 ± 0.04	1.32 ± 0.06
	98th	0.35 ± 0.03	1.18 ± 0.02
	99th	0.28 ± 0.02	1.24 ± 0.02
	99.9th	0.76 ± 0.03	0.96 ± 0.01
	mean*	0.28 ± 0.03	1.25 ± 0.03

ACPD
15, 2157–2196, 2015

Table 2. Occurrence of convective and stratiform events. Number of quadrants of Germany classified as convective (C) or stratiform (S) in the 3 hourly synoptic observations. The maximum possible values for the two years and for all four quadrants is 23360. This number reduces by about half for the seasonal data, and again by half for the sub-regions of Germany.

area	type	year	summer	winter
all	S	1358	206	1152
all	C	1537	1270	267
north	S	761	103	658
north	C	741	590	151
south	S	597	103	494
south	C	796	680	116

ACPD
15, 2157–2196, 2015

Figure 1. Data used in the analysis. Map of Germany with the synoptic stations (red crosses) and the radar locations and approximate range (gray circles). Dashed black lines indicate the division of the domain into quadrants.

ACPD
15, 2157–2196, 2015

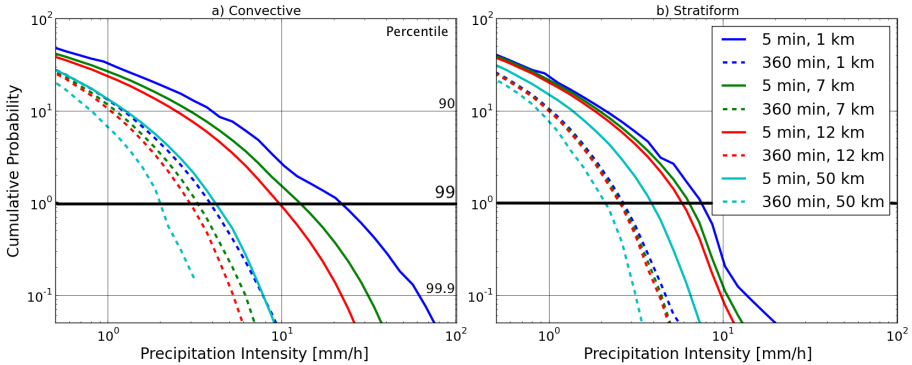

Figure 2. Cumulative probability density functions of precipitation intensities. All of Germany for the years 2007–2008, aggregated at different horizontal and temporal resolutions. **(a)** convective events; **(b)** stratiform events.

ACPD
15, 2157–2196, 2015

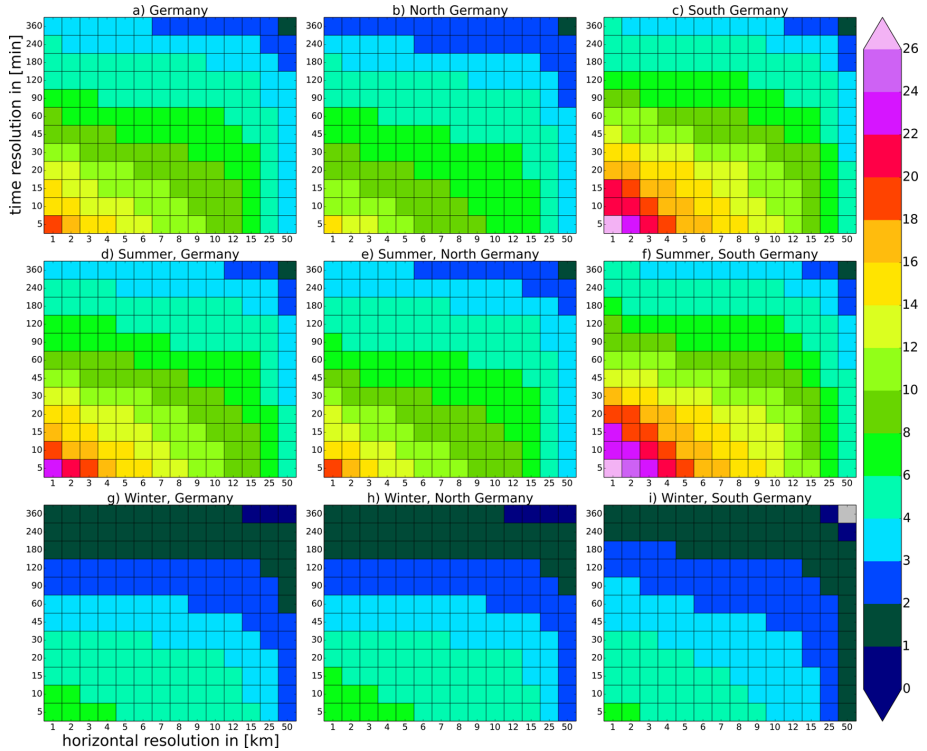

Figure 3. Convective extremes as function of resolution. The 99th percentile of convective precipitation intensities, aggregated over different parts of Germany for the years 2007–2008, on different horizontal (horizontal axis) and temporal (vertical axis) resolutions: Entire year **(a–c)**, summer season **(d–f)** and winter season **(g–i)**. All of Germany **(a, d, g)**, North Germany **(b, e, h)**, South Germany **(c, f, i)**; Intensities given in mm h^{-1}.

ACPD
15, 2157–2196, 2015

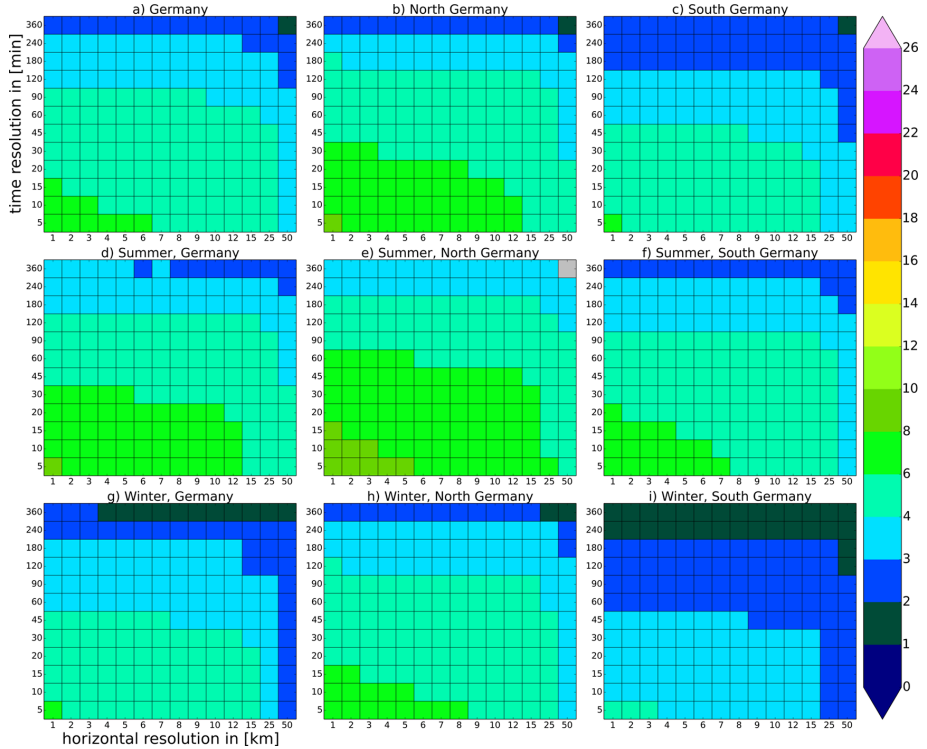

Figure 4. Stratiform extremes as function of resolution. Otherwise similar to Fig. 3.

ACPD
15, 2157–2196, 2015

Temporal and spatial scaling impacts on extreme precipitation

B. Eggert et al.

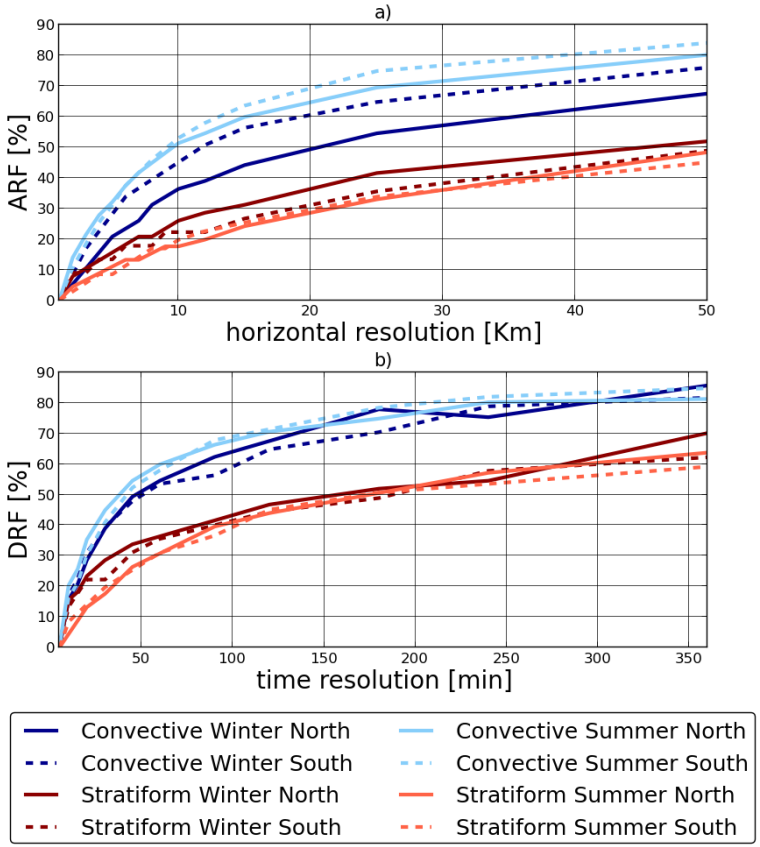

Figure 5. Area and duration reduction factors. (a) area reduction factors at 5 min temporal resolution. **(b)** duration reduction factors (DRF) for 1 km × 1 km spatial resolution in percent, for convective (blue) and stratiform (red) precipitation. Data shown for the summer and winter seasons and north and south Germany.

ACPD
15, 2157–2196, 2015

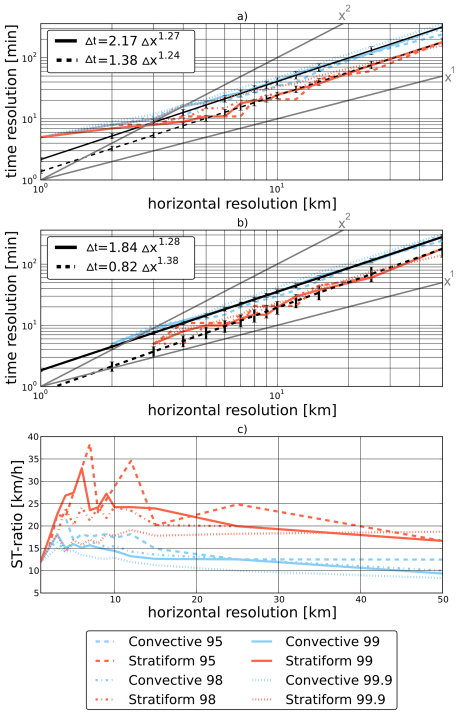

Figure 6. Consistent spatial and temporal resolutions. Δt derived using Eq. (5) for different values of Δx for convective (blue) and stratiform (red) precipitation extremes at the 95th, 98th, 99th and 99.9th percentiles. Black lines are least square fit of $\Delta t = a \times \Delta x^b$ with the fitting parameters a and b for the 99th percentile. Errorbars indicate the standard deviation of parameter estimates. Gray lines show $\Delta t \sim \Delta x$ and $\Delta t \sim \Delta x^2$, respectively. **(a)** Initial resolutions $\Delta t_0 = 5$ min, $\Delta x_0 = 1$ km. **(b)** $\Delta t_0 = 5$ min, and aggregated spatial resolutions $\Delta x_0 = 2$ km (convective) and $\Delta x_0 = 3$ km (stratiform). **(c)** ST ratio (Eq. 7) for both precipitation types for Germany over the entire year.

ACPD
15, 2157–2196, 2015

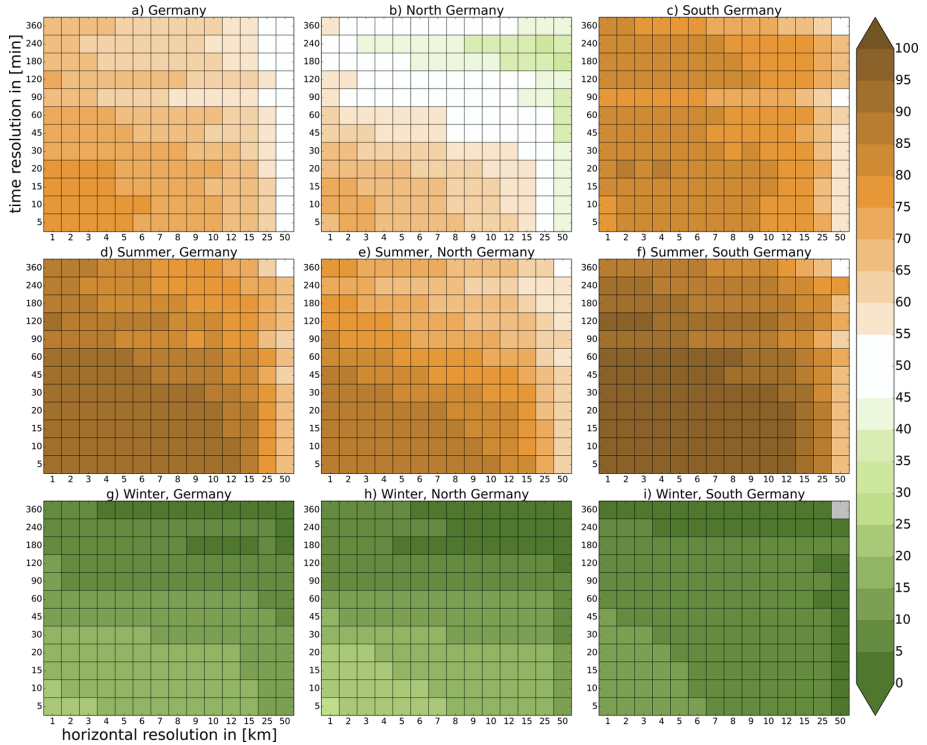

Figure 7. Convective dominance as function of resolution including dry periods. The ratio of the number of convective precipitation events with precipitation intensities larger or equal threshold intensity. Threshold intensity is defined as the 99th percentile of total precipitation intensities over the different parts of Germany for the years 2007–2008. Panels otherwise as in Fig. 3.

ACPD
15, 2157–2196, 2015

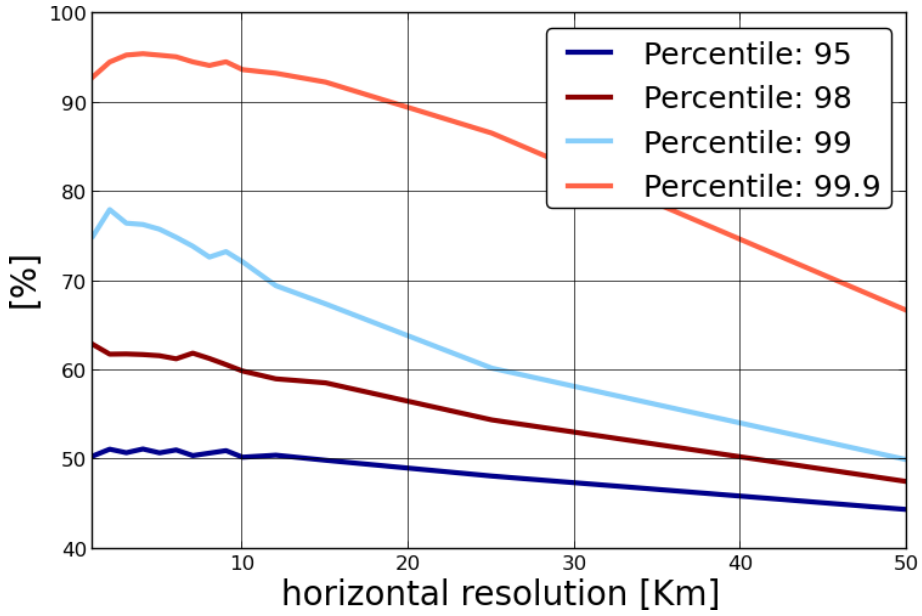

Figure 8. Convective dominance vs. horizontal resolution. The ratio of the number of convective precipitation events with precipitation intensities larger or equal the labeled percentile of total precipitation intensities over entire Germany for the years 2007–2008. The data is aggregated to 5 min temporal and different horizontal resolutions.

ACPD
15, 2157–2196, 2015

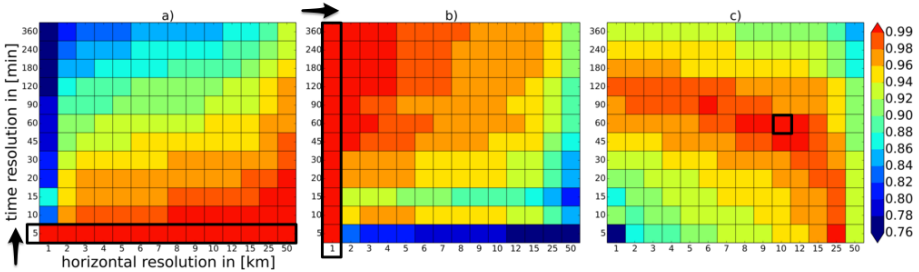

Figure 9. PDF overlap for convective precipitation intensity. All of Germany for the years 2007–2008, aggregated to different horizontal (horizontal axis) and temporal (vertical axis) resolutions. **(a)** PDF overlap of each horizontal resolution between every temporal resolution and the 5 min data. **(b)** PDF overlap of each temporal resolution between every horizontal resolution and the 1 km data. **(c)** PDF overlap of each horizontal and temporal resolution compared to the 10 km, 60 min data.

ACPD
15, 2157–2196, 2015

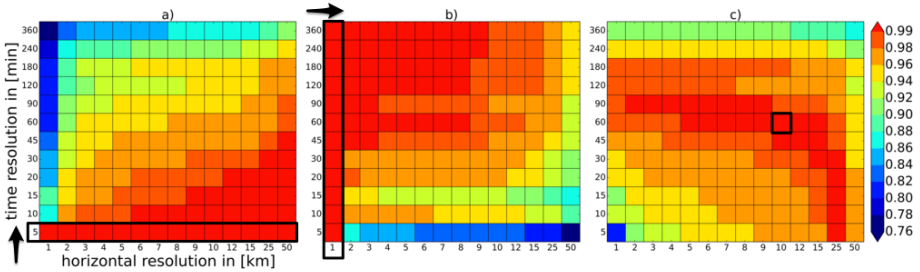

Figure 10. PDF overlap of stratiform precipitation intensity. Otherwise similar to Fig. 9.

ACPD
15, 2157–2196, 2015